Proceedings of the
Annual Stability Conference
Structural Stability Research Council
San Antonio, Texas, March 19-22, 2024

Influence of residual stresses on the cross-section stability of WF shapes

Lucile Gérard[1], Nicolas Boissonnade[2]

Abstract

Steel WF or I-shapes are usually fabricated by either hot-rolling or welding. Both manufacturing processes produce residual stresses that affect the stability behavior and resistance, namely at the member level (e.g., flexural or lateral torsional buckling). Yet, at the cross-sectional level, design provisions typically ignore the influence of residual stresses and propose identical sets of equations for hot-rolled and for welded sections.

This paper numerically evidences that this should be improved and investigates how much more detrimental welded residual stresses patterns can be in comparison to hot-rolled ones, in various contexts. The results of detailed non-linear shell F.E. simulations on various geometries, slenderness, material grades and load cases are reported and analyzed, and recommendations for code improvements are proposed.

1. Introduction

Cross-sectional resistance of steel profiles is typically governed by material yielding, instability (local buckling), imperfections and their multiple interactions. Cross-sections with the most compact shapes (i.e., made of thick plates) usually exhibit plastic capacities – attainment of yield stress in all fibers –, whereas cross-sections with more slender geometries experience early local buckling so that their carrying capacity may be significantly affected. Plastic or compact sections – Class 1-2 sections within Eurocode 3's nomenclature – therefore are associated to plastic verifications, while slender shapes (Class 4 sections) require an adequate treatment of local buckling effects, usually through the use of the Effective Width Method ((European Committee for Standardization (CEN), 2018a), (American Institute of Steel Construction, 2022), (CSA-S16, 2019)). In the latter case, especially for geometries of moderate slenderness, imperfections play a key role within the plasticity-instability interaction. In this respect, residual stresses typically affect peak load: the more detrimental the residual stresses pattern, the lower the capacity.

Different production processes lead to different residual stresses patterns. For example, hot-rolled (Figs. 1-4) or welded (Fig. 5) residual stresses patterns remain very classical for carbon steel. For many years, research investigations involving measurements of imperfections have been reported. (see for example (Greiner et al., 2009), (Thiébaud, 2014), (Davids & Hancock, 1986), (Chick & Rasmussen, 1999) and Fig. 1). Many of the available experimental results

[1] PhD, INGENOVA, <lucile.gerard1@gmail.com>
[2] Professor, Laval University, <nicolas.boissonnade@gci.ulaval.ca>

trace back to test series realized at Lehigh University in the 60's and 70's ((Tebedge et al., 1973), (Alpsten & Tall, 1969)). They reflect the difficulty to obtain accurate experimental measurements of residual stresses. Different techniques exist, the most classical ones being the strip-cutting, the use of strain gauges or the whole drilling method. As an obvious requirement, residual stresses patterns must ensure self-equilibrium on the section that is not acted by any external force (Bruneau et al., 2011); yet, reports on measurements typically indicate that experimental patterns lay usually (quite) far from this, further evidencing the difficulty to measure residual stresses experimentally.

Amplitudes and distributions of residual stresses can be shown to depend on various aspects, such as the cross-section geometry or the manufacturing procedures and temperatures employed during fabrication ((Bruneau et al., 2011), (Petersen, 2012), (Ziemian, 2010)). Fabrication processes also evolved in the last decades (e.g., cold-straightening is known to reduce residual stresses levels) and may in some cases result in much lower intensity patterns, cf. (Ge & Yura, 2019). However, recent measurements ((Clarin, 2004), (Quach, 2005), (Yuan et al., 2014), (Hadjioannou et al., 2013), (Gardner & Cruise, 2009), (Szalai & Papp, 2005), (Spoorenberg et al., 2013), (Wang et al., 2012)) still report high amplitudes of residual stresses for hot-rolled profiles (being from regular or high strength steel) and welded residual stresses patterns still remain with the highest values and the most detrimental effects. Also, no major changes towards new "updated" types of residual stresses can be observed in design standards ((American Institute of Steel Construction, 2022), (CSA-S16, 2019), (ECCS - TC8, 1984)).

Although major design codes may not directly give recommendations on the residual stresses distributions to consider, they provide various resistance equations that differ depending on the manufacturing process. For example, the resistance of columns to flexural buckling in Eurocode 3 (EC3, 2005) relies on a series of 5 buckling curves which depend on the fabrication process of the column, e.g., hot-rolled, welded, cold-formed (for tubes), … Residual stresses are known to have their most detrimental influence at intermediate slenderness (Maquoi & Rondal, 1978), (Bruneau et al., 2011), (Petersen, 2012).

Even though an indirect account for residual stresses is proposed within several resistance checks, the cross-section resistance of steel profiles still remains indifferent to the manufacturing process, while it clearly should for slender and moderately slender sections. The present paper relies on advanced F.E. models to evidence in which extent this disregard may affect carrying capacities at the cross-section level. Section 2 first briefly summarizes well-known and commonly-used residual stresses distributions that have further been implemented in shell F.E. models described in Section 3. Finally, Section 4 provides results for various residual stresses patterns on section subjected to either simple compression or major-axis ending; comparisons on the resistance of hot-rolled and welded sections are also presented.

2. Brief overview of recommendations for residual stresses patterns

2.1 Hot-rolled I-shapes

The present paragraph aims at proposing a brief review of well-known recommendations for residual stresses patterns for hot-rolled section shapes – for more details, one may check the quite extensive paper of Abambres & Quach (Abambres & Quach, 2016). In this respect, one may refer to the recognized measurements performed at Lehigh University in the 1970's (Alpsten & Tall, 1969), (Tebedge et al., 1973), (Tebedge et al., 1971), that helped paving the way for further such investigations. Careful and well documented results served as a basis for code implementation and in particular served in the derivation of column buckling curves. Fig. 1 proposes such typical residual stresses patterns, which are representative of the manufacturing reality back then. Further comparable proposals may also be mentioned here,

such as the ones suggested by ECCS in 1984 (ECCS - TC8, 1984) or Ketter (Ketter, 1958), cf. Fig. 2.

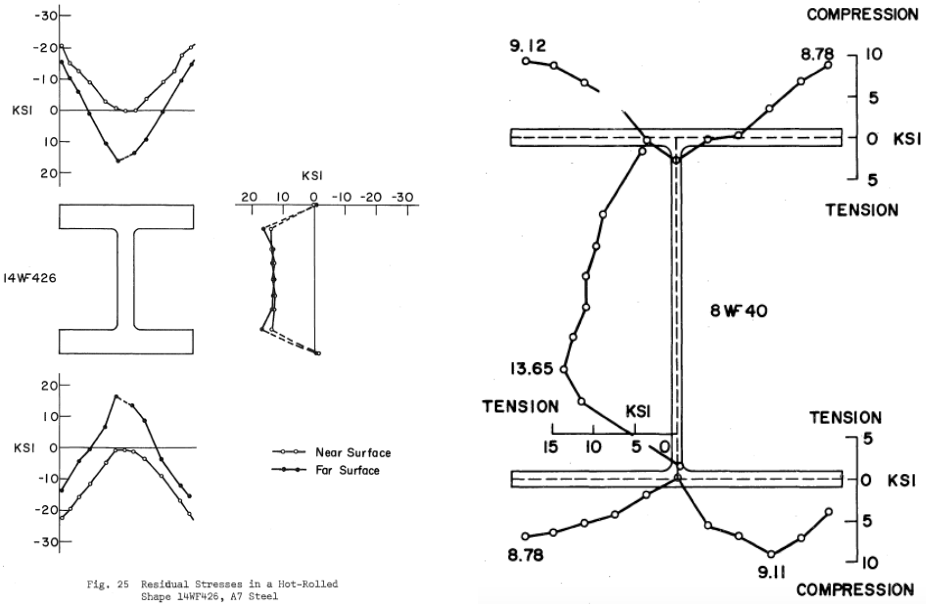

Figure 1: Residual stresses measurements on a hot-rolled specimen – (a) From (Alpsten & Tall, 1969) and (b) From (Kim & Daniels, 1970).

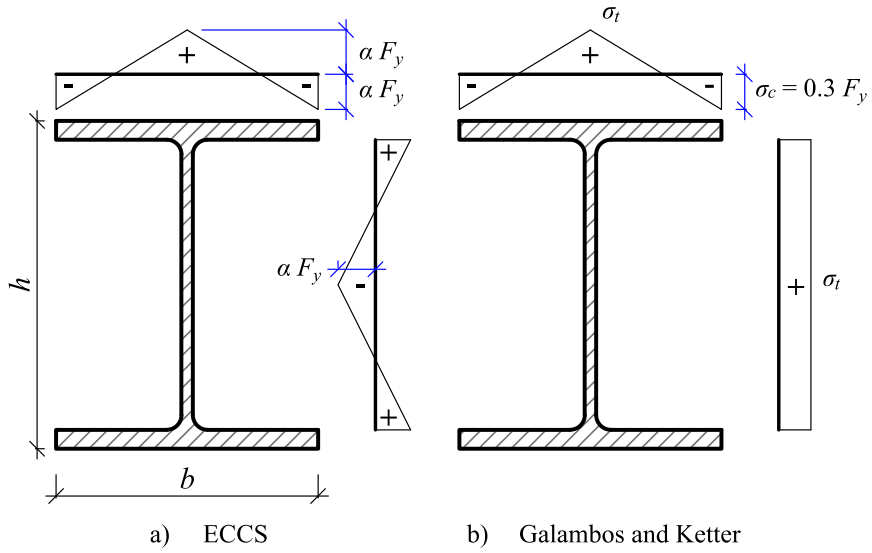

Figure 2: Residual stresses patterns for hot-rolled sections from a) ECCS (ECCS - TC8, 1984), b) Ketter (Ketter, 1958).

Besides usual "triangular distributions, other authors such as Young (Fig. 3) or the German Standards Association (Deutsche Institut fur Normung, 1990) further proposed parabolic patterns (Fig. 4), slightly more favorable than their triangular counterparts. Unlike in Ketter or in the ECCS pattern, the residual stresses amplitudes proposed by Young were not made dependent on the material yield strength. Fig. 4 exhibits further parabolic distributions for hot-rolled sections proposed in (Deutsche Institut fur Normung, 1990), which include residual stresses amplitudes being a portion of a 235 *MPa* reference stress. The use of a fraction of 235 *MPa* for hot-rolled sections stems from recommendations resulting from the measurements realized throughout years 1960-1970: a unique steel grade S250W was available back then and further experimental series on higher steel grades showed that residual stresses amplitudes did not increase with the material yield strength (Tebedge et al., 1971).

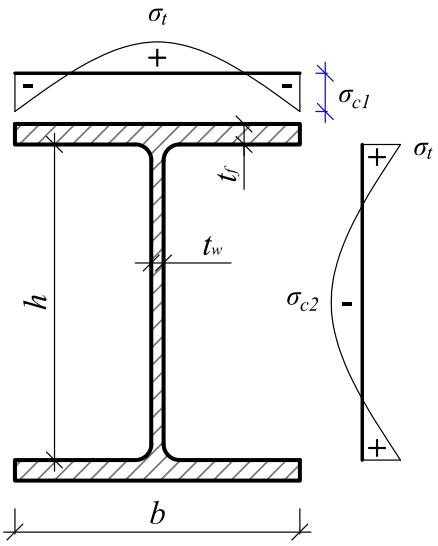

Figure 3: Residual stresses pattern for hot-rolled sections from Young (Young, 1975).

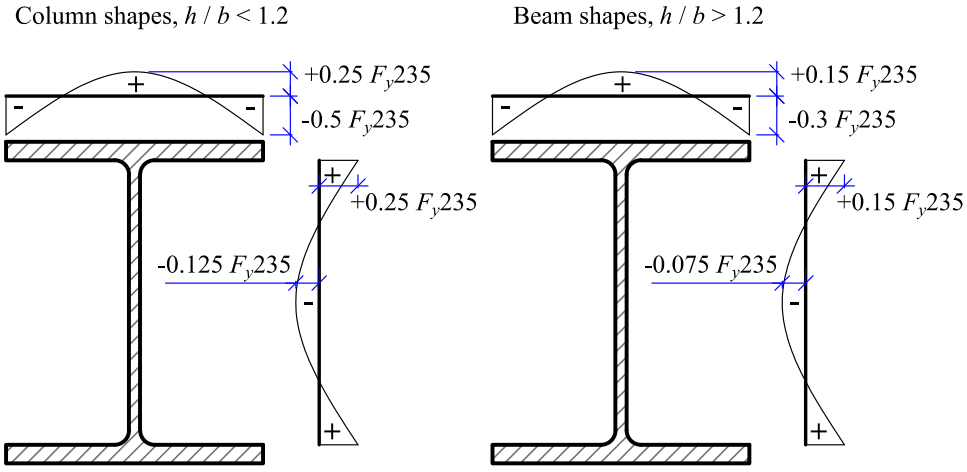

Figure 4: Residual stresses pattern for hot-rolled sections ((Deutsche Institut fur Normung, 1990)).

2.2 Welded I-shapes

Uneven cooling may as well occur as a result of welding plates together to build the section (see Fig. 5) and/or flame cutting the plates to the desired dimensions. Residual stresses as high as the yield limit can be reached on areas near welds where the material has been highly heated, or at the edges of plates fabricated by means of flame cutting. Fig. 5a corresponds to the associated ECCS (1984) proposal ((ECCS - TC8, 1984)), where the steel yield characteristic strength f_{yk} is reached on welded areas.

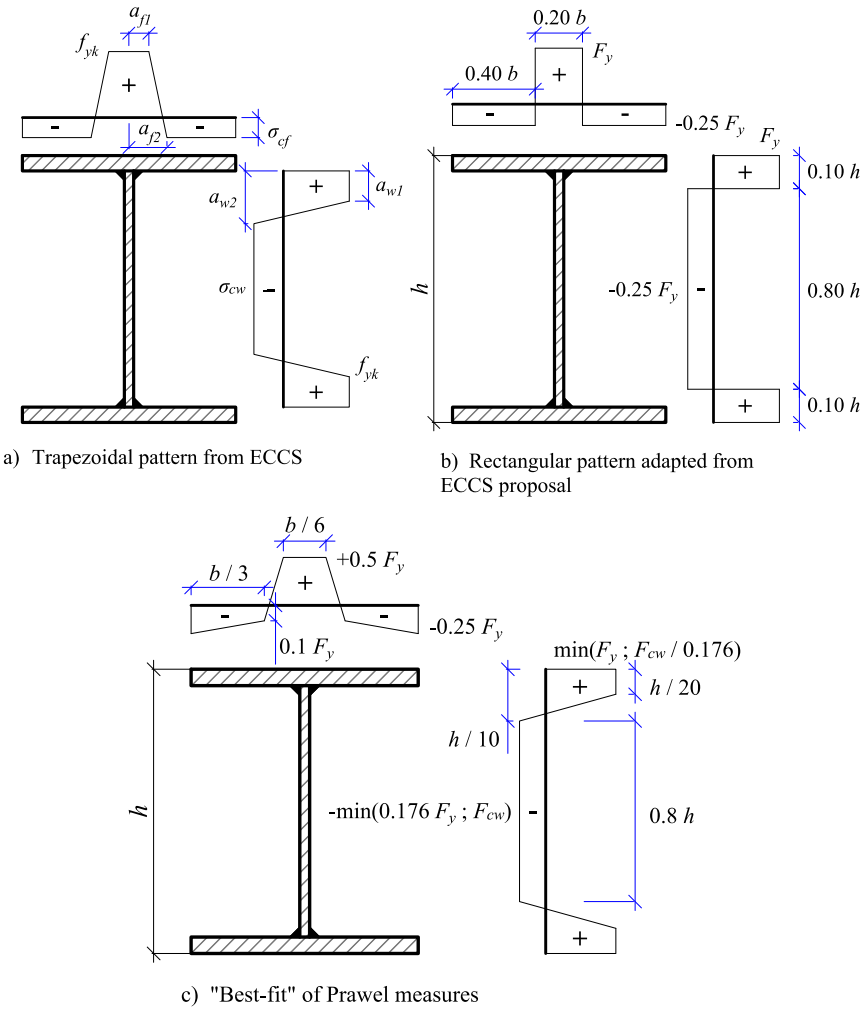

a) Trapezoidal pattern from ECCS

b) Rectangular pattern adapted from ECCS proposal

c) "Best-fit" of Prawel measures

Figure 5: Residual stresses patterns for welded sections.

3. Development of F.E. models

3.1 Basic features and assumptions

Numerical simulations were performed by means of Finite Element software FINELg, developed in collaboration between the University of Liège and Greish design office ((FINELg, 2011)). FINELg has been used successfully for many structural engineering applications as well as in many numerical parametric studies where several comparisons with test data allowed for an effective validation ((Nseir, 2015), (Hayeck, 2016)). In the present studies, analyses such as Linear Buckling Analyses (L.B.A.) and Geometrically and Materially Non-linear with Imperfections Analyses (G.M.N.I.A.) were carried out. Elements employed were quadrangular 4 nodes shell Finite Elements based on Kirchoff's theory in bending that also accounted for membrane behavior. Total Corotational Lagrangian Formulation taking due account of the current deflected configurations of elements and 7 integration points through the thickness were considered using Gauss numerical integration schemes. L.B.A. calculations resorted to the so-called "subspace iteration method", and G.M.N.I.A. analyses were based on state of the art numerical techniques and strategies: pure Newton-Raphson iterative scheme with out of balance residual corrections associated to the arc-length method and automatic loading strategies up to peak load and beyond. A reliable and computationally efficient mesh was adopted following preliminary mesh density studies on both hot-rolled and welded F.E. models (Gérard, 2020).

For hot-rolled sections, a specific modelling of the web to flange area (see Fig. 6) was accounted for. Firstly, the fillet zones were replaced by a beam element placed at the center of gravity of the two corner zones, whose area compensated for the absence of the fillets (Boissonnade & Somja, 2012). Moreover, inherently to a shell modelling, an overlap between plate elements occurs at the web/flange intersection. Accordingly, the extra beam element properties were set including the overlap influence so that the actual profiles geometrical characteristics (area, inertia…) were matched (Boissonnade & Somja, 2012). In addition, since the actual web-to-flange geometry exhibits important rigidity resulting from the fillets, additional truss elements were introduced into the F.E. model (Fig. 6), so as to maintain this region unaffected by potential local buckling in the adjacent plates.

As for welded sections, for which the welds do not provide a significant restraint to local buckling of the web and flanges, no such truss elements were introduced at the web to flange junction; additional beam elements were excluded from welded models as well.

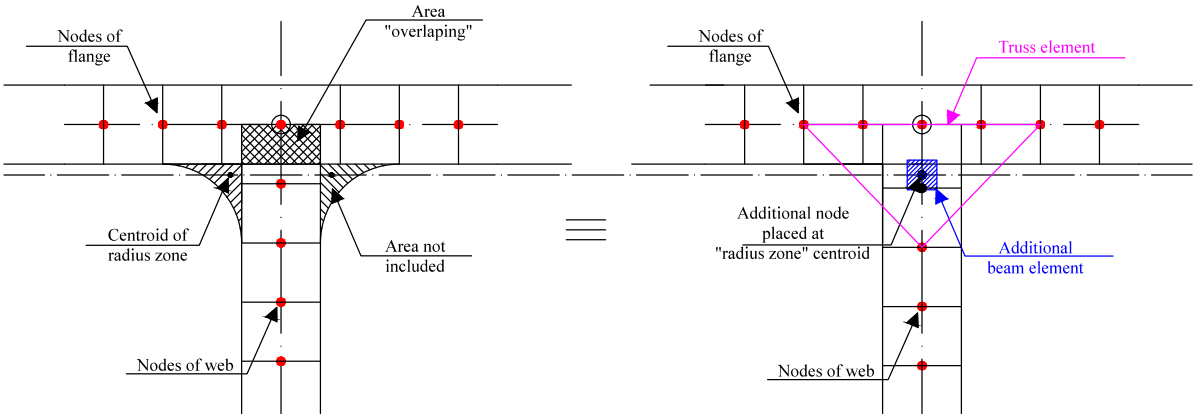

Figure 6: Web-to-flange intersection modelling of a hot-rolled section.

The stress strain constitutive law adopted and represented on Fig. 7 classically includes a plastic plateau followed by suitable strain hardening regions. The strain hardening slope as well as the 10% maximum strain were chosen according to previous studies ((Hayeck, 2016)) and recommendations ((ECCS Technical Committee, 1976)). The material law shown on Fig. 7 is suitable for standard yield limits such as $F_y = 235\ MPa$ and $F_y = 460\ MPa$ which were considered in the current study.

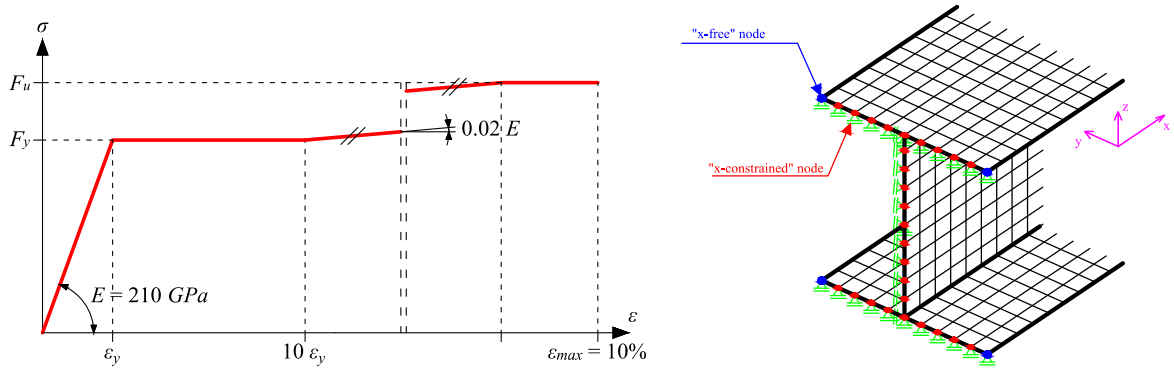

Figure 7: (a) Material properties – (b) Kinematic constraints in the F.E. model.

Classic ideal fork support conditions were applied at both ends (u_y, u_z and θ_x fixed, see axes defined in Fig. 7) and axial displacement u_x was constrained at one end section. Moreover, kinematic linear constraints were considered for end sections to fulfil beam theory assumptions. In order to allow for a maximum number of 4 global degrees of freedom (i.e., cross section

experiencing u_x, θ_y, θ_z and warping displacements as a whole), the displacements of all "x constrained nodes", which are highlighted on Fig. 7, were imposed as a combination of the 4 deformation modes.

Loading was applied at the 4 flanges tip nodes by means of suitable sets of nodal forces, for all load cases. Inherently to the kinematic constraint conditions, the end sections were prevented from concentration of stresses and Bernoulli-like assumptions in bending "plane sections remain plane" were consequently fulfilled – more details on these aspects may be found in (Gérard, 2020).

Within the present F.E. parametric studies, a large range of geometries has been considered, covering compact to very slender sections, for both IPE (beam shapes) and HEA (column shapes) sections. In order to include more slender sections, two geometries with 30% reduced thickness compared to the original sections' dimensions were invented: IPES and HEAS, where "S" refers to more slender shapes: The following geometries were considered under pure compression and pure major axis bending:

- IPE140 (h = 140 *mm*; b = 73 *mm*; t_w = 4.7 *mm*; t_f = 6.9 *mm*; h / b = 1.92);
- IPE400 (h = 400 *mm*; b = 180 *mm*; t_w = 8.6 *mm*; t_f = 13.5 *mm*; h / b = 2.22);
- IPES (h = 800 *mm*; b = 220 *mm*; t_w = 10 *mm*; t_f = 19 *mm*; h / b = 3.57);
- HEA160 (h = 152 *mm*; b = 160 *mm*; t_w = 6 *mm*; t_f = 9 *mm*; h / b = 0.95);
- HEA600 (h = 590 *mm*; b = 300 *mm*; t_w = 13 *mm*; t_f = 25 *mm*; h / b = = 1.96);
- HEAS (h = 300 *mm*; b = 300 *mm*; t_w = 6 *mm*; t_f = 10 *mm*; h / b = 1.0).

For numerical modelling convenience, the length of each member was chosen sufficiently short to avoid the occurrence of global buckling but long enough to reduce the influence of edge conditions. Moreover, the member length was made dependent on the local geometrical imperfection pattern to ensure the desired number of half waves and sinusoidal period (see Table 1 and Section 3.3 for more details).

It is important to mention that previously to any numerical series, the suitability of the F.E. model was verified against experimental data. The F.E. model was indeed compared to experimental results gathered from test series carried out on hot-rolled and welded H profiles. A very good agreement between experimental and numerical results was achieved, assessing the reliability of the numerical model ((Gérard, 2020), (Gérard et al., 2021)).

3.2 Geometrical imperfections

Various types of local geometrical imperfections were considered. An extensive analysis of their influence on the load carrying capacity of open sections is presented in (Gérard et al., 2019). Geometrical imperfections were introduced into the F.E. model by means of either appropriate modifications of nodes coordinates through adequate sinusoidal functions or based on the 1st local buckling shape. For each way of introducing these imperfections, several cases were considered. With respect to imperfections accounted for through sinusoidal functions, different numbers of initial half-waves, amplitudes and periods were studied.

Table 1 summarizes the various sets of geometrical imperfections considered in this paper, as per the various sinusoidal shapes considered. The name of each case presented in Table 1 respectively describes the number of half-waves, the half-wave length and the amplitude of the sinusoid used to produce the initial deformed shape. As an example, a case denoted "3hw / P_avg / A_pp_200" refers to an initial imperfect shape characterized by the presence of 3 half-waves, a half-wave length equal to the average between the web buckling length a_w and the flange buckling length a_f, and an amplitude applied respectively to each plate characteristic buckling length divided by 200 (Gérard et al., 2019). Further to differences in dimensions, plate buckling lengths in flanges and web may differ according to the manufacturing process

considered. In the particular case of hot-rolled sections, plate buckling lengths a_w and a_f were defined as $a_w = h - 2\,t_f - 2\,r$ and $a_f = b - t_w - 2\,r$ ("flat lengths") where h refers to the whole height of the profile, while for welded sections, $a_w = h - t_f$ and $a_f = b$ were used. Consequently, a_{avg} represents the average between the flange and web plate buckling lengths.

Table 1: Characteristics associated to each cross-section considered in the present investigations.

Case	Half-Period	Amplitude web	Amplitude flange
a) 3hw / P_avg / A_pp_200	a_{avg}	a_w / 200	a_f / 200
b) 2hw / P_avg / A_pp_200	a_{avg}	a_w / 200	a_f / 200
c) 3hw / P_f / A_pp_200	a_f	a_w / 200	a_f / 200
d) 3hw / P_w / A_pp_200	a_w	a_w / 200	a_f / 200
e) 3hw / P_avg / A_avg_200	a_{avg}	a_{avg} / 200	a_{avg} / 200
f) 3hw / P_avg / A_f_200	a_{avg}	a_f / 200	a_f / 200
g) 3hw / P_avg / A_w_200	a_{avg}	a_w / 200	a_w / 200
h) 3hw / P_avg / A_pp_100	a_{avg}	a_w / 100	a_f / 100
i) 3hw / P_avg / A_pp_400	a_{avg}	a_w / 400	a_f / 400
j) -hw / P_pp / A_pp_200[1]	Period per plate	a_w / 200	a_f / 200

[1] -hw means that different numbers of sine-waves have been adopted on the flanges and web.

The use of the 1st local buckling mode shape obtained through Linear Buckling Analyses (L.B.A.) represents one of the most common methods to account for geometrical initial imperfections. Several values of amplitude applied to adequately scale the eigenmode shape were considered. Table 2 specifies the values of initial amplitudes adopted in each case. "Amplitude *x*" refers to the amplitude applied along the member axis (*x*-axis) while "amplitude *y*" (web) and "amplitude *z*" (flange) represent the transverse amplitudes considered on the *y* and *z* directions, respectively.

Table 2: Values of amplitudes applied to scale the 1st buckling mode shape.

Case	Amplitude *x*	Amplitude *y*	Amplitude *z*
A_avg_100	a_{avg} / 100	a_{avg} / 100	a_{avg} / 100
A_avg_200	a_{avg} / 200	a_{avg} / 200	a_{avg} / 200
A_avg_400	a_{avg} / 400	a_{avg} / 400	a_{avg} / 400
A_pp_100	a_{avg} / 100	a_w / 100	a_f / 100
A_pp_200	a_{avg} / 200	a_w / 200	a_f / 200
A_pp_400	a_{avg} / 400	a_w / 400	a_f / 400

3.3 Material imperfections

Two different residual stresses patterns were considered for hot-rolled sections: the triangular residual stresses shape displayed on Fig. 2a and the parabolic pattern described on Fig. 4. As for welded sections, two different residual stresses patterns were studied as well: the rectangular pattern of Fig 8a and the trapezoidal one from Fig. 8b. The rectangular residual stresses pattern was adapted from the trapezoidal pattern suggested by ECCS ((ECCS - TC8, 1984)). It presents a constant compressive stresses amplitude on the web and flanges, regardless of the section's geometry.

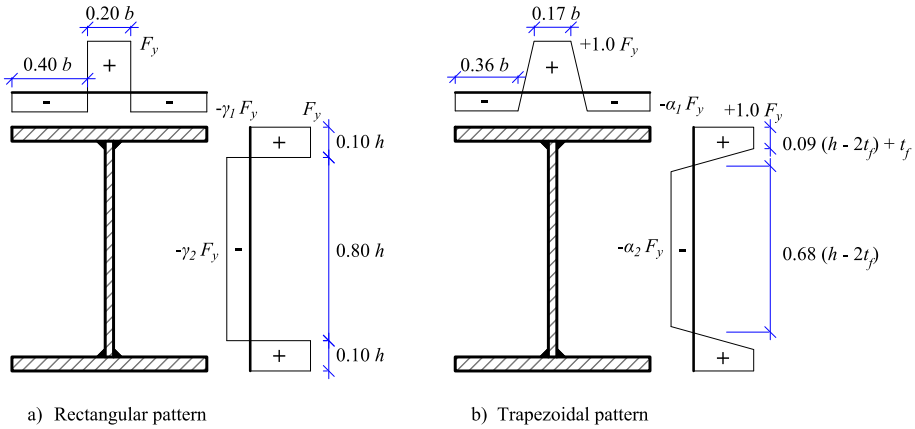

Figure 8: Residual stresses patterns for welded sections.

The trapezoidal pattern was adapted from (Lindner, 1998) to respect a self-equilibrium condition in each plate, as former ones. Coefficients α_1 and α_2 can be calculated from the section dimensions under the assumption of plate-per-plate equilibrated residual stresses patterns. Accordingly, parameter α_2 depends on the section's geometry and may be higher than the usual 0.25 value. Eqs. (1) and (2) definitions of parameters γ_1, γ_2, α_1 and α_2 were assumed for the welded patterns.

$$\gamma_1 = 0.25 \qquad \gamma_2 = 0.25 \tag{1}$$

$$\alpha_1 = \frac{9}{31} \qquad \alpha_2 = \frac{0.125 \cdot h + 0.75 \cdot t_f}{0.375 \cdot h - 0.75 \cdot t_f} \tag{2}$$

If such residual stresses are to be considered in the F.E. model alongside local geometrical imperfections, Eurocode 3 Part 1.5 ((European Committee for Standardization (CEN), 2018b)) indicates the possibility to apply a reduction of 30% to secondary imperfections if a leading imperfection is selected (either a geometrical or a material one). Although the Standard recommends adopting certain patterns and amplitudes for geometrical imperfections, it does not provide any guidance with respect to the adoption of a suitable residual stresses pattern. Yet, this situation recently improved through the still-informative Part 1.14 dedicated to design assisted by finite element analysis (CEN/TC 250, 2021).

4. Influence of residual stresses on I-shapes cross-section resistance

4.1 Hot-rolled profiles

Firstly, the influence of hot-rolled residual stresses patterns on the local load carrying capacity is studied. In the following, "triangular_F_y = 235 *MPa*" and "triangular_F_y actual" refer to results obtained with triangular residual stresses patterns, whereas "parabolic_F_y = 235 *MPa*" and "parabolic_F_y actual" are related to parabolic ones. "F_y actual" describes residual stresses shapes where the maximum residual stress depends on the *actual* yield limit while "F_y = 235 *MPa*" relates to maximum residual stresses being *a fraction of* 235 *MPa*.

Fig. 9 and Fig. 10 first present results obtained for the local behavior of I-sections and H-sections under compression, respectively. The horizontal axis on the $\lambda_L = f(\chi_L)$ graphs refers to the *local* (L) relative slenderness λ_L (see Eq. (3)), while the vertical axis represents the *local* reduction factor χ_L, which is defined in Eq. (4) ((Boissonnade et al., 2017)). The *local* slenderness λ_L characterizes the ratio of the section plastic resistance to its *local* buckling load. Expressions in Eq. (3) correspond to the definition of the local slenderness λ_L for pure compression and pure bending load cases. They refer to $N_{cr,L}$ which is the *local* axial critical

buckling load of a perfect section, and to $M_{cr,L}$ which stands as the *local* critical buckling bending moment of an ideal section.

$$\bar{\lambda}_L = \sqrt{\frac{N_{pl}}{N_{cr,L}}} \qquad \bar{\lambda}_L = \sqrt{\frac{M_{pl}}{M_{cr,L}}} \tag{3}$$

Then, definitions of the local reduction factor χ_L for a section under axial compression or major axis bending, are given in Eqs. (4), where N_{ult} and M_{ult} correspond to ultimate local capacities while N_{pl} and M_{pl} refer to plastic capacities. χ_L shall therefore be seen as a direct measure of the ultimate (design) resistance: a value $\chi_L = 0.75$ means that only 75% of the plastic capacity may be reached at the ultimate (design) level owing to local buckling effects, i.e., early local buckling takes out 25% of the plastic capacity you may expect from a section unaffected by local instabilities.

$$\chi_L = \frac{N_{ult}}{N_{pl}} \qquad \chi_L = \frac{M_{ult}}{M_{pl}} \tag{4}$$

Figs. 9 and 10 – as well as many subsequent ones – also generically plot the following references:

- The horizontal dashed line $\chi_L = 1.0$ which refers to the plastic resistance, i.e., no influence of imperfections nor buckling;
- The hyperbolic dashed line $\chi_L = 1 / \lambda_L$ describing Von Karman's equation for the design of an ideal plate free of imperfections;
- The well-known Winter curve for plate design – as being calibrated from isolated plates' test data, it includes the effects of imperfections;
- A "Kettler proposal" additional curve (Kettler, 2008) which originates from a study on the cross section capacity of semi compact H sections, and may serve as a recent reference.

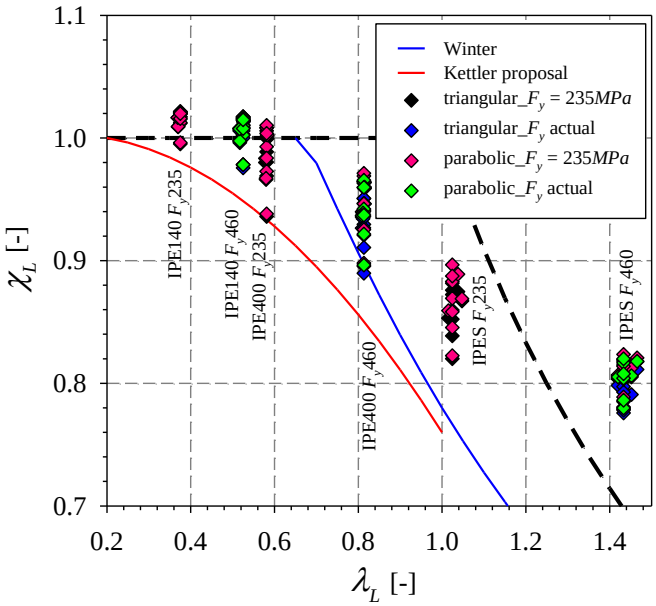

Figure 9: Hot-rolled I sections under pure compression.

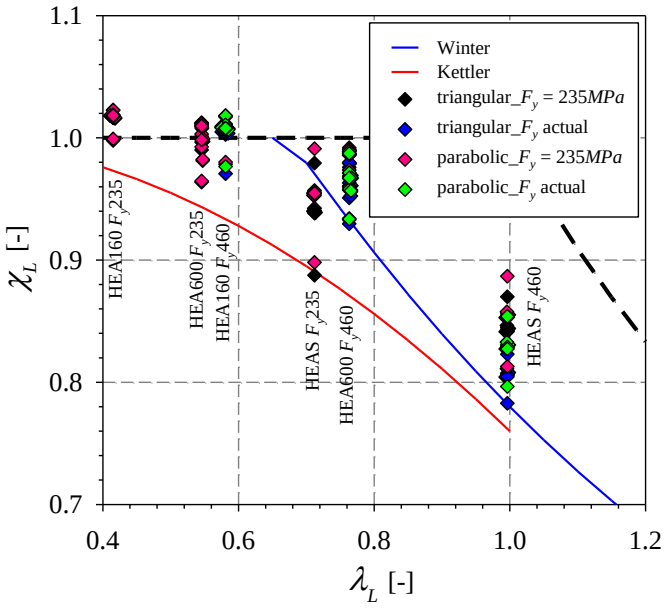

Figure 10: Hot-rolled H-sections under pure compression.

As a global trend observed on the figures, compact sections are seen to exhibit very similar resistances, regardless of the different residual stresses patterns introduced, which is mostly attributed to their lower sensitivity to imperfections. On Fig. 9, an important discrepancy in the results is observed at a slenderness $\lambda_L \approx 1.0$. This disparity is due to the influence of both the residual stresses chosen and the variations in geometrical imperfections; extreme cases show up to 10% discrepancy. Furthermore, results obtained for each residual stresses pattern for very slender sections such as IPES with $\lambda_L \approx 1.45$ display negligible differences, as a result of a lesser sensitivity to imperfections for this range of slenderness.

To better visualize differences in resistance for a given section, Fig. 11 exhibits histograms of the same results for selected I and H-sections under both load cases investigated in the study. The graphs were obtained for each residual stresses pattern with a specific geometrical imperfection corresponding to case a) 3hw / P_avg / A_pp_200 specified previously. For each specimen studied, Fig. 11 provides the corresponding local reduction factor on the vertical axis.

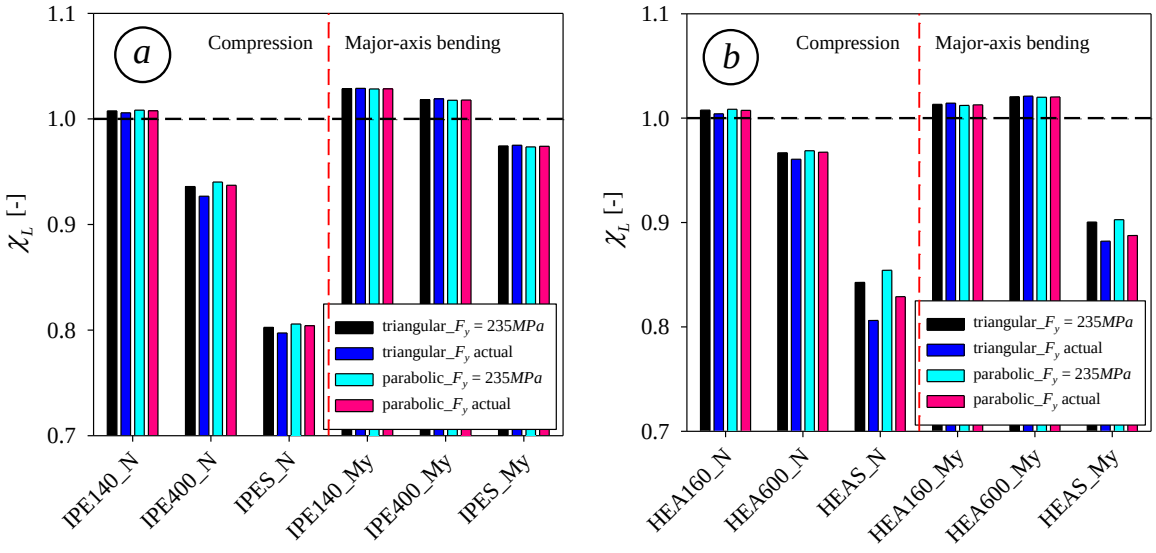

Figure 11: Hot-rolled residual stresses pattern influence on (a) I-sections and (b) H-sections – S460 steel.

As expected, Fig. 11 points out that that when the actual yield limit is used instead of a conventional one (e.g., F_y = 235 *MPa*) for sections made of higher steel grades such as S460, a lower resistance is obviously attained. As a matter of fact, sections made of S460 steel achieve a larger maximum residual stress if the maximum residual stress is based on a fraction of the yield stress (e.g., 460 *MPa*) rather than on the conventional value. Under increasing loading, the various fibers composing a section in S460 steel therefore reach their plastic limit earlier, and, hence, yielding spreads quicker, involving earlier buckling and ultimately, a relative earlier failure. Consequently, the following observations may be further outlined:

- Compact sections whose applied residual stresses pattern relies on the *actual* yield stress achieve important deformations earlier and reach lower ultimate strengths than the ones with residual stresses pattern based on a *conventional* strength F_y = 235 *MPa*;
- The earlier occurrence of yielding if higher residual stresses are applied on more slender sections such as IPE400 and HEAS ones results in premature buckling and triggers geometrical non-linear effects earlier.

Moreover, Fig. 11 allows to observe that the parabolic residual stresses pattern seems to lead to slightly higher resistances than the triangular residual stresses pattern, especially within sections of intermediate slenderness such as IPE400 and HEAS. As a matter of fact, the influence of the variations in residual stresses patterns is more pronounced since this range of slenderness is more sensitive to the presence of imperfections. A more detrimental residual stresses pattern therefore affects the occurrence of yielding and buckling which are both involved in the failure of sections with intermediate slenderness.

For a deeper analysis of the discrepancies produced with the various patterns and values of residual stresses considered, Table 3 presents succinct statistical results for sections under axial compression. This table enables to assess further remarks and exposes the major discrepancies. Moreover, since ratios were determined for similar geometrical imperfections, the influence of their shape and amplitude can be excluded.

Table 3: Statistical comparison between hot-rolled residual stresses patterns for sections under pure compression.

	$\chi_{L,\ triangular\_Fy\ =\ 235\ MPa}$ / $\chi_{L,\ triangular\_Fy\_actual}$		$\chi_{L,\ parabolic\_Fy\ =\ 235\ MPa}$ / $\chi_{L,\ parabolic\_Fy\_actual}$		$\chi_{L,\ triangular\_Fy\_actual}$ / $\chi_{L,\ parabolic\_Fy\_actual}$	
	I-shape	*H*-shape	*I*-shape	*H*-shape	*I*-shape	*H*-shape
Maximum [%]	101.8	**105.7**	100.8	**103.8**	99.9	99.9
Minimum [%]	100.1	100.1	100.0	100.0	98.1	**96.4**
Average [%]	100.7	101.9	100.3	101.1	99.2	98.7
Std. dev. [%]	0.53	**1.91**	0.22	**1.37**	0.57	**1.08**
Number of results	30	30	30	30	30	30

Columns $\chi_{L,\ triangular\_Fy\ =\ 235\ MPa}$ / $\chi_{L,\ triangular\_Fy\_actual}$ and $\chi_{L,\ parabolic\_Fy\ =\ 235\ MPa}$ / $\chi_{L,\ parabolic\_Fy\_actual}$ show the influence of the maximum residual stress used, for a similar pattern shape. Then, the 3rd column, $\chi_{L,\ triangular\_Fy\_actual}$ / $\chi_{L,\ parabolic\_Fy\_actual}$, points out the influence of the pattern's shape.

As expected and previously highlighted, the divergence from a pattern shape to another remains very reasonable (resp. 0.57% and 1.08% of standard deviation obtained for I and H-shapes in compression). The difference provided with the maximum residual stresses used is reasonable as well – see the 1st and 2nd columns. Ratios present an overall standard deviation below 2%.

Bold values in Table 3 point out the maximum differences encountered throughout the available data. The maximum difference (5.7%) is obtained for an H-type section under pure compression. This divergence is reached for a triangular pattern shape between the two different maximum residual stresses considered. Sections HEAS lead to the major differences seen on

the tables. Together with IPE140, HEAS presents the thinner plates compared to the other specimens. While maximum amplitudes of 0.30 F_y are applied to IPE140 geometries in accordance with ECCS's residual stresses recommendations, residual stresses as high as 0.50 F_y are applied to HEAS. Higher residual stresses precipitate the development and consequent expansion of yielded areas. Combined with lower plates thicknesses, the fibers adjacent to the early yielded zones may be "activated faster" to carry further loading.

As a conclusion, the discrepancies reported on Fig. 9 to Fig. 11 are not significant enough to decide which residual stresses pattern shall take precedence for hot-rolled sections. Both parabolic and triangular residual stresses shapes provide ultimate resistances in reasonable agreement. Although the parabolic shape leads to slightly higher local resistances, the difference with the triangular one is not statistically significant. Jönsson and Stan (Jönsson & Stan, 2017) carried out a similar investigation but focused on such influences on columns member strengths. They observed a maximum of 4% and 12% difference between triangular and parabolic residual stresses shapes influence for an IPE160 and HEB300, respectively. Considering only the triangular pattern, Valeš and Stan (Valeš & Stan, 2017) investigated the influence of the presence of residual stresses on the member strength of beams and observed up to 7% differences in average of ultimate capacities reached with and without residual stresses, while Szalai and Papp (Szalai & Papp, 2005) reported up to 9% difference for column member strengths. Nonetheless, such studies were restricted to a limited number of sections and additional section shapes shall be investigated to obtain a more representative dataset.

With respect to the maximum residual stresses used, negligible differences were highlighted in the present study but at intermediate section slenderness, such difference was seen to reach up to 12% for a H-shape with F_y = 690 *MPa*, according to Jönsson et al. (Jönsson & Stan, 2017). Nonetheless, since no references in literature justify the attainment of residual stresses as high as a fraction of the actual yield stress for hot-rolled sections, the use of the reference stress 235 *MPa* is considered to represent the most reasonable option.

4.2 Welded profiles

Again through $\lambda_L - \chi_L$ axes, Fig. 12 exhibits the results obtained from numerical simulations on welded I-sections (Fig. 12a) and H-sections (Fig. 12b). Histograms presenting the results obtained for welded sections with respect to a specific case of geometrical imperfections – case a) 3hw / P_avg / A_pp_200 – are shown in Fig. 13. "Rectangular" refers to sections whose residual stresses pattern corresponds to the rectangular one suggested in Fig. 8a, while "trapezoidal" relates to the trapezoidal pattern, cf. Fig. 8b. For both patterns, a maximum residual stress corresponding to the *actual* yield limit was considered since residual stresses as high as the yield limit are usually reached in the thermally affected areas.

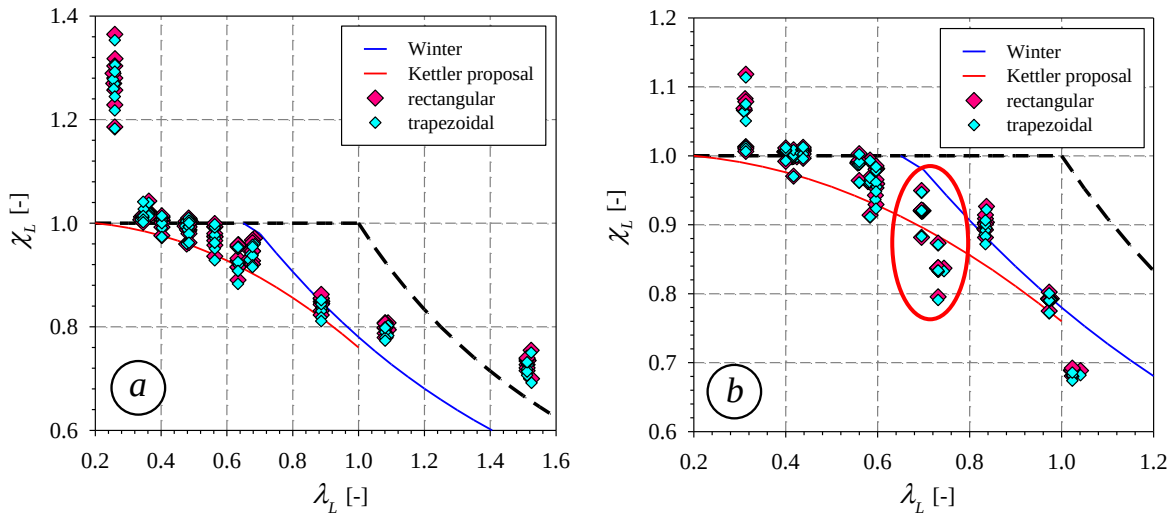

Figure 12: (a) Welded I-sections and (b) H-sections strengths under N and M_y.

Albeit the rectangular and trapezoidal patterns do not generally lead to significant differences (see Fig. 12), the behavior of H-sections shows an increased disparity (see red ellipse on Fig. 12b) that results from the influence of more detrimental/favorable geometrical imperfection amplitudes. A maximum difference of 9% for a similar geometry, load case and yield limit is observed. The histograms in Fig. 13 further point out minor differences between results. For the intermediate section IPE400 under pure compression, where the highest differences are observed, the resistances reached with both residual stresses patterns remain notably similar.

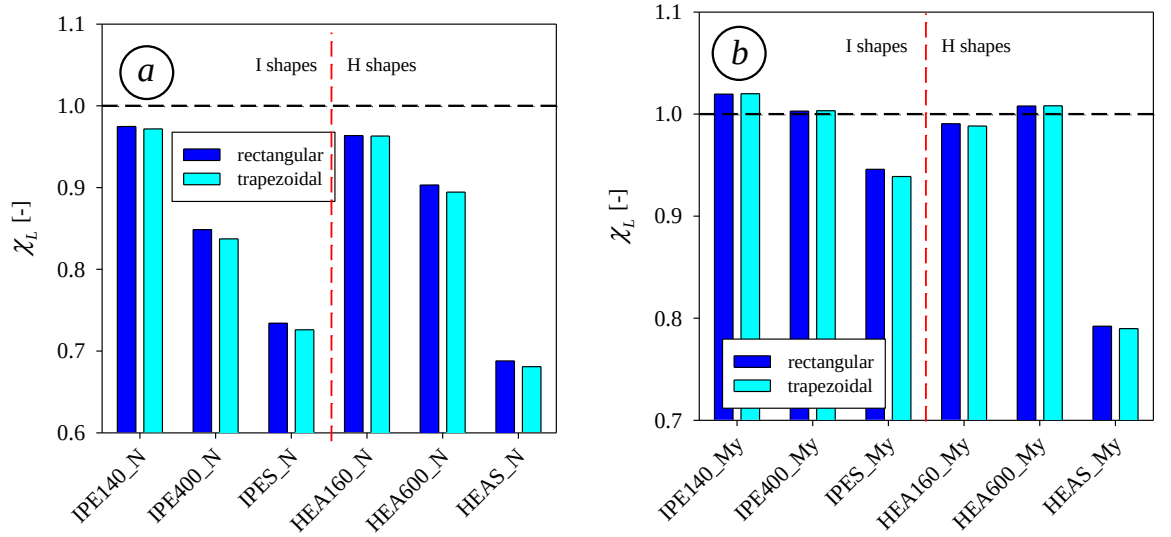

Figure 13: Welded residual stresses pattern influence on I and H-sections – S460 steel (a) N (b) M_y.

Table 4: Statistical comparison between rectangular and trapezoidal patterns.

$\chi_{L,\,rectangular}$ / $\chi_{L,\,trapezoidal}$	*I*-shape	*H*-shape
Maximum [%]	101.5	101.1
Minimum [%]	97.5	96.4
Average [%]	100.5	100.3
Standard deviation [%]	0.6	0.5
Number of results	108	108

Table 4 offers a statistical summary which confirms the observations made previously: standard deviations as well as average values for both I and H-shapes show that most of the results present less than 1% difference between the two residual stresses shapes.

As for those patterns' influence on the member strength, Couto and Vila Real (Couto & Vila Real, 2019), who investigated the influence of the rectangular pattern on the global strength of beams, made some comparisons with other residual stresses shapes influences. The authors pointed out the presence of a strength's drop – typically at intermediate slenderness – associated to the rectangular pattern and the trapezoidal one suggested by ECCS (ECCS - TC8, 1984), while the "best-fit" of Prawel measures used by Subramanian and White (Subramanian & White, 2017) was seen to result in higher strength curves. Experimental tests on welded slender sections could be needed to further assess the exactness of such numerically-predicted responses.

4.3 Comparison between hot-rolled and welded results

Table 5 provides a comparison of local reduction factors χ_L reached with (i) the hot-rolled parabolic residual stresses pattern using the *reference* yield limit $F_y = 235\ MPa$ and with (ii) the welded rectangular pattern based on the *actual* limit for the maximum residual stress reached.

Table 5: Statistical comparison between hot-rolled and welded patterns for H-shapes.

$\chi_{L,\ Welded} / \chi_{L,\ Hot\text{-}rolled}$	N	M_y
Maximum [%]	98.6	104.4
Minimum [%]	78.0	86.2
Average [%]	91.9	95.6
Standard deviation [%]	6.1	4.1
Number of results	60	60

As is well-known, the table shows that residual stresses in welded sections lead to substantial resistance reductions compared to hot-rolled residual stresses. The lowest average value (91.9%) and highest standard deviation (6.1%) are of course achieved for sections loaded in axial compression. These results may be explained by the increased slenderness reached for this load case: indeed, most of the local relative slenderness values obtained with N lie in the range of λ_L where imperfections influence the behavior, while many of the λ_L reached for M_y cases correspond to more compact cross sections, thus the larger differences.

Fig. 14 exhibits the $\chi_{L,\ Welded} / \chi_{L,\ Hot\text{-}rolled}$ ratio of the local reduction factors obtained with the welded and hot-rolled residual stresses patterns, as a function of the local relative slenderness $\lambda_{L,\ Hot\text{-}rolled}$, for hot-rolled cross sections. It is worth noting here that up to 10% difference in the relative slenderness value were noticed between hot-rolled and welded sections, due to the absence of rigid web-to-flange areas in the welded models. Consequently, correspondence in λ_L values is somewhat lost as $\lambda_{L,\ Hot\text{-}rolled}$ values are usually smaller than their $\lambda_{L,\ Welded}$ counterparts.

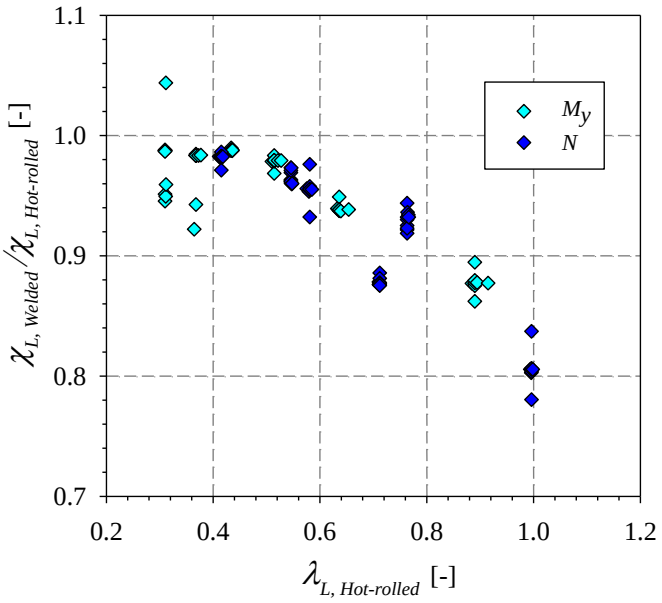

Figure 14: Ratio between welded and hot-rolled sections local reductions factors, for H-shapes.

As a general observation, the figure emphasizes the important influence of welded residual stresses in the drop of resistance for high values of $\lambda_{L,\,Hot\text{-}rolled}$ as a decreasing $\chi_{L,\,Welded}$ / $\chi_{L,\,Hot\text{-}rolled}$ is observed when $\lambda_{L,\,Hot\text{-}rolled}$ increases – drops in relative resistance up to 20%. Besides, for sections under M_y, tensile residual stresses add to the tensile stresses arising from bending. Since some residual stresses are already as high as the yield stress, the very first load increment applied is immediately followed by permanent strains in the tensile zones and yielding can be observed to spread quickly. The early influence of yielding, combined with local buckling, considerably decreases the ultimate resistance of welded sections. On the other hand, for sections under axial compression, the detrimental influence of welded residual stresses results from the wider area where compressive residual stresses are present, compared to hot-rolled patterns.

Since welded profiles exhibit lower resistances compared to hot-rolled ones, the inclusion of welded residual stresses into a numerical model is crucial and a reliable pattern shape needs to be used. Nonetheless, results presented in paragraph 4.2 point out minor discrepancies between the rectangular and trapezoidal shapes with a maximum difference of 3.6%. Accordingly, both patterns may be equivalently considered and implemented in F.E. models.

5. Recommendations for F.E. modelling

The current paper leads to the following observations and recommendations for the introduction of residual stresses in F.E. models:

- A parabolic pattern with a maximum residual stress of 235 *MPa* may represent the most suitable choice for hot-rolled column H-shapes, on the basis of experimental data;
- While the triangular pattern highlights greater agreement with residual stresses measurements on beam IPE shapes, it does not lead to significant differences from resistance predictions obtained with the parabolic pattern (see Section 4). These differences are even lower for beam shapes than column shapes (Gérard, 2020);
- Although the parabolic pattern is slightly more favorable than the triangular one, both shapes may be very acceptable for the F.E. modelling of hot-rolled sections;
- Even though the use of the *actual* yield stress for hot-rolled sections leads to lower resistances than when a *reference* stress of 235 *MPa* is considered, negligible differences were highlighted. Because the attainment of a fraction of the actual yield

stress for hot-rolled sections is not reported in experimental measurements, the use of a portion of the reference stress 235 *MPa* represents the most reasonable option;
- In case of welded sections, negligible differences were observed between results obtained with a rectangular or with a trapezoidal pattern; the rectangular pattern certainly is the easiest to implement in practice, though.

Hence, the parabolic residual stresses pattern (see Fig. 4) with a maximum residual stress based on a *reference* stress of 235 *MPa* is suggested for hot-rolled sections. Besides, the rectangular residual stresses pattern (see Fig. 8) with a maximum residual stress corresponding to the actual yield stress shall be recommended for welded sections.

Eventually, one shall not forget that nowadays, steel profiles are sometimes subjected to rotary straightening, leading to quite different distributions of residual stresses (Ge & Yura, 2019). Further experimental measurements on profiles manufactured accordingly shall allow for closer estimations of residual stresses amplitudes and better prediction of ultimate strengths owing to more appropriate patterns.

6. Conclusions

Through extensive non-linear shell F.E. analyses, the present paper further evidences the need to account for different sets of design rules between hot-rolled and welded WF sections, at the *cross-section level* – which is not the case in major standards presently. Various residual stresses patterns were investigated, on both welded and hot-rolled manufactured profiles; in particular, the influence of both the distribution and maximum residual stress were addressed. Eventually, the paper conveniently summarizes guidelines/recommendations on the most appropriate and reasonable residual stresses patterns to consider within F.E. non-linear analyses, i.e., a parabolic residual stresses pattern for hot-rolled profiles and a rectangular distribution for welded sections.

5. Bibliography

Abambres, M., & Quach, W.-M. (2016). Residual stresses in steel members : A review of available analytical expressions. *International Journal of Structural Integrity*, *7*(1), 70-94. https://doi.org/10/gg3wzh

Alpsten, G. A., & Tall, L. (1969). *RESIDUAL STRESSES IN HEAVY WELDED SHAPES*. 66.

American Institute of Steel Construction. (2022). *Specification for Structural Steel Buildings*.

Boissonnade, N., Hayeck, M., Saloumi, E., & Nseir, J. (2017). An Overall Interaction Concept for an alternative approach to steel members design. *Journal of Constructional Steel Research*, *135*, 199-212. https://doi.org/10/gbkrf8

Boissonnade, N., & Somja, H. (2012). Influence of imperfections in FEM modeling of lateral torsional buckling. *Proceedings of the Annual Stability Conference, Structural Stability Research Council, Grapevine, Texas, April 18, 21*.

Bruneau, M., Uang, C.-M., & Sabelli, R. (2011). *Ductile design of steel structures*. McGraw Hill.

CEN/TC 250. (2021). *Eurocode 3 : Design of steel structures—Part 1-14 : Design assisted by finite element analysis*.

Chick, C. G., & Rasmussen, K. J. (1999). Thin-walled beam-columns. I : Sequential loading and moment gradient tests. *Journal of Structural Engineering*, *125*(11), 1257-1266.

Clarin, M. (2004). *High strength steel : Local buckling and residual stresses*. Lulea University of Technology.

Couto, C., & Vila Real, P. (2019). On the interaction between local and lateral-torsional buckling of I-shaped slender section beams. *Proceedings of the Annual Stability Conference of the Structural Stability Research Council (SSRC)*.

CSA-S16. (2019). *Design of Steel Structures*. CAN/CSA-S16:19. Canadian Standards Association (CSA), Mississauga, Ont.

Davids, A. J., & Hancock, G. J. (1986). Compression Tests of Short Welded I-Sections. *Journal of Structural Engineering*, *112*(5), 960-976. https://doi.org/10/dfr4np

Deutsche Institut fur Normung. (1990). *DIN 18800 Teil 1 : Stahlbauten, Bemessung und Konstruktion*.

EC3. (2005). *EN 1993-1-1 : Eurocode 3—Design of steel structures—Part 1-1 : General rules and rules for buildings*. European Committee for Standardization (CEN).

ECCS - TC8. (1984). *Ulitmate Limit state Calculation fo Sway Frames with Rigid Joints* (First Edition). ECCS.

ECCS Technical Committee. (1976). *Manual on Stability of Steel Structures*.

European Committee for Standardization (CEN). (2018a). *prEN 1993-1-1 : Eurocode 3—Design of steel structures—Part 1-1 : General rules and rules for buildings*. https://standards.globalspec.com/std/14327633/PREN%201993-1-1

European Committee for Standardization (CEN). (2018b). *prEN 1993-1-5 : Eurocode 3—Design of steel structures—Part 1-5 : Plated structural elements*. https://standards.globalspec.com/std/14500117/PREN%201993-1-5

FINELg. (2011). *FINELg User's Manual*.

Gardner, L., & Cruise, R. B. (2009). Modeling of Residual Stresses in Structural Stainless Steel Sections. *Journal of Structural Engineering*, *135*(1), 42-53. https://doi.org/10.1061/(ASCE)0733-9445(2009)135:1(42)

Ge, X., & Yura, J. (2019). The strength of rotary-straightened steel columns. *Proceedings of the Annual Stability Conference of the Structural Stability Research Council (SSRC)*.

Gérard, L. (2020). *Contribution to the design of steel I and H-sections members by means of the Overall Interaction Concept* [PhD thesis]. Laval University.

Gérard, L., Li, L., Kettler, M., & Boissonnade, N. (2019). Recommendations on the geometrical imperfections definition for the resistance of I-sections. *Journal of Constructional Steel Research*, *162*, 105716. https://doi.org/10/gg3w2v

Gérard, L., Li, L., Kettler, M., & Boissonnade, N. (2021). Steel I-sections resistance under compression or bending by the Overall Interaction Concept. *Journal of Constructional Steel Research*, *182*, 106644. https://doi.org/10/gjj6wg

Greiner, R., Kettler, M., Lechner, A., Freytag, B., Linder, J., Jaspart, J. P., Boissonnade, N., Bortolotti, E., Weynand, K., & Ziller, C. (2009). SEMI-COMP : Plastic member capacity of semi-compact steel sections–a more economic design. *European Commission, Research Fund for Coal and Steel, Luxembourg: Office for Official Publications of the European Communities*.

Hadjioannou, M., Douthe, C., & Gantes, C. J. (2013). Influence of cold bending on the resistance of wide flange members. *International Journal of Steel Structures*, *13*(2), 353-366. https://doi.org/10.1007/s13296-013-2013-6

Hayeck, M. (2016). *Development of a new design method for steel hollow section members resistance* [PhD thesis]. University of Applied Sciences of Western Switzerland - Fribourg, University of Liège, Saint-Joseph University Beirut.

Jönsson, J., & Stan, T.-C. (2017). European column buckling curves and finite element modelling including high strength steels. *Journal of Constructional Steel Research*, *128*, 136-151. https://doi.org/10.1016/j.jcsr.2016.08.013

Ketter, R. L. (1958). *THE INFLUENCE OF RESIDUAL STRESS ON THE STRENGTH OF STRUCTURAL MEMBERS*. 15.

Kettler, M. (2008). *Elastic-plastic cross-sectional resistance of semi-compact H- and hollow sections* [PhD thesis]. Graz University of Technology, Styria, Austria.

Kim, S., & Daniels, J. (1970). *Experiments on restrained columns permitted to sway*. Fritz Engineering Laboratory.

Lindner, J. (1998). *Stahlbauten : Erläuterungen zu DIN 18800 Teil 1 bis Teil 4*.

Maquoi, R., & Rondal, J. (1978). Mise en équation des nouvelles courbes européennes de flambement. *Construction métallique*, *15*(1), 17-30.

Nseir, J. (2015). *Development of a new design method for the cross-section capacity of steel hollow sections* [PhD thesis]. University of Applied Sciences of Western Switzerland - Fribourg, University of Liège, Saint-Joseph University Beirut.

Petersen, C. (2012). *Stahlbau : Grundlagen der Berechnung und baulichen Ausbildung von Stahlbauten*. Springer-Verlag.

Quach, W. M. (2005). *Residual stresses in cold-formed steel sections and their effect on column behaviour*. The Hong Kong Polytechnic University.

Spoorenberg, R. C., Snijder, H. H., Cajot, L.-G., & May, M. S. (2013). Experimental investigation on residual stresses in heavy wide flange QST steel sections. *Journal of Constructional Steel Research*, *89*, 63-74. https://doi.org/10.1016/j.jcsr.2013.06.009

Subramanian, L., & White, D. W. (2017). Resolving the disconnects between lateral torsional buckling experimental tests, test simulations and design strength equations. *Journal of Constructional Steel Research, 128,* 321-334. https://doi.org/10.1016/j.jcsr.2016.08.009

Szalai, J., & Papp, F. (2005). A new residual stress distribution for hot-rolled I-shaped sections. *Journal of Constructional Steel Research*, *61*(6), 845-861. https://doi.org/10/b2j2kj

Tebedge, N., Alpsten, G., & Tall, L. (1971). Measurement of residual stresses. A study of methods. *Fritz Laboratory Reports*, 9.

Tebedge, N., Alpsten, G., & Tall, L. (1973). Residual-stress measurement by the sectioning method : A procedure for residual-stress measurements by the sectioning method is described. Two different hole-drilling methods were performed and the results are compared. *Experimental Mechanics*, *13*(2), 88-96. https://doi.org/10/fm94hf

Thiébaud, R. (2014). *Résistance au déversement des poutres métalliques de pont—PhD Thesis*.

Valeš, J., & Stan, T.-C. (2017). FEM Modelling of Lateral-Torsional Buckling Using Shell and Solid Elements. *Procedia Engineering*, *190*, 464-471. https://doi.org/10.1016/j.proeng.2017.05.365

Wang, Y.-B., Li, G.-Q., & Chen, S.-W. (2012). Residual stresses in welded flame-cut high strength steel H-sections. *Journal of Constructional Steel Research*, *79*, 159-165. https://doi.org/10.1016/j.jcsr.2012.07.014

Young, B. (1975). Residual stresses in hot-rolled members. *IABSE reports of the working commissions*.

Yuan, H. X., Wang, Y. Q., Shi, Y. J., & Gardner, L. (2014). Residual stress distributions in welded stainless steel sections. *Thin-Walled Structures*, *79*, 38-51. https://doi.org/10.1016/j.tws.2014.01.022

Ziemian, R. D. (2010). *Guide to stability design criteria for metal structures*. John Wiley & Sons.